Journal of Solid State Chemistry 182 (2009) 2707–2715

Contents lists available at ScienceDirect

Journal of Solid State Chemistry

journal homepage: www.elsevier.com/locate/jssc

Five novel transition metal coordination polymers with 2D/3D framework structure based on flexible H_2tzda and ancillary ligand bpe

Yu-Ting Wang [a,b], Yan Xu [b], Yao-Ting Fan [b,*], Hong-Wei Hou [b]

[a] Department of Chemistry, Henan Institute of Education, Henan 450014, PR China
[b] Department of Chemistry, Zhengzhou University, Zhengzhou, Henan 450052, PR China

ARTICLE INFO

Article history:
Received 27 April 2009
Received in revised form
9 July 2009
Accepted 12 July 2009
Available online 18 July 2009

Keywords:
Flexible dicarboxylate ligands
Coordination polymers
Transition metal
Hydrothermal synthesis
Luminescent property
Magnetic behavior

ABSTRACT

Five new transition metal coordination polymers based on H_2tzda and co-ligand bpe, $\{[M(\text{tzda})(\text{bpe})]\cdot H_2O\}_n$ [M = Zn(**1**), Cd(**2**), Mn(**3**), Co(**4**)] and $[Ni_2(\text{tzda})_2(\text{bpe})_2(H_2O)]_n$ (**5**) [H_2tzda = (1,3,4-thiadiazole-2,5-diyldithio)diacetic acid, bpe = 1,2-bis(4-pyridyl)ethane], have been hydrothermally synthesized and structurally characterized. Compounds **1–4** feature a 2D-layered architecture generated from $[M(\text{tzda})]_n$ moiety with double-chain structure cross-linking bpe spacers. However, the conformations bpe adopts in **3** and **4** are different from those in **1** and **2** due to the rotation of C–C single bond in bpe. Polymer **5** exhibits an interesting 3D porous framework with 2-fold interpenetration, in which intriguing 1D double helix chains are observed. The photoluminescence properties of **1** and **2** in the solid-state at room temperature are investigated. In addition, variable-temperature magnetic data show weak antiferromagnetic behavior in **3–5**.

1. Introduction

In the past decades, considerable attention has been devoted to the metal–organic frameworks (MOFs) constructed by metal ions and polycarboxylate-type ligands owing to their structural diversity, intriguing architectures and topologies, as well as wide potential applications as functional materials [1–6]. Significant progress has been achieved in this field, however, among the numerous reported studies, great efforts have been focused on rigid aromatic carboxylate ligands such as 1,4-benzenedicarboxylate [7], 1,2,4,5-benzenetracarbaxyalte [8], and 1H-benzimidazole-5,6-dicarboxylic acid [9]. In contrast, coordination polymers assembled by metal salts with flexible ones are not well done so far due to the difficulties in predicting the resulted framework structures, though they may induce novel topologies and unique properties owing to their flexibility and conformation freedoms [10,11]. On the other hand, the multidentate N-donor ligands with certain spaces, form example, 4,4′-bipyridine (bpy), 1,2-bis(4-pyridyl)ethane (bpe) and its analogues, have been extensively employed as auxiliary ligands in the construction of extended structures since they can satisfy the coordination needs of metal atoms and consequently generate more meaningful architectures [12–18]. Thus, taking the above factors into account, the combination of metal ions and bridging ligands containing flexible polycarboxylates and dipyridyl pillars can allow the formation of extended coordination networks with beautiful aesthetics and useful functional properties.

Recently, a series of coordination polymers of rare earth and transition metal ions with flexible dicarboxylate ligand H_2tzda, such as $[Ln_2(\text{tzda})_3(H_2O)_5]_n$ [Ln = Er, Pr, Nd, Eu] and $[M(\text{tzda})(H_2O)_4]_n$ [M = Co, Ni and Zn] [H_2tzda = (1,3,4-thiadiazole-2,5-diyldithio)diacetic acid] have been reported in our lab [19,20]. H_2tzda has been proved to be an encouraging organic linker in these compounds, exhibiting a variety of flexible coordination forms. To gain more information about the coordination information of metal coordination polymer based on flexible ligand H_2tzda, now our attention has been paid to the assembly of novel transitional metal framework structures with H_2tzda and flexible auxiliary ligand bpe [1,2-bis(4-pyridyl)ethane]. Herein, we report the preparation and properties of five new coordination polymers of transition metal ions based on flexible H_2tzda and co-ligand bpe, namely, $\{[M(\text{tzda})(\text{bpe})]\cdot H_2O\}_n$ [M = Zn(**1**), Cd(**2**), Mn(**3**), Co(**4**)] and $[Ni_2(\text{tzda})_2(\text{bpe})_2(H_2O)]_n$ (**5**). X-ray analyses show that all of these complexes exhibit 2D or 3D frameworks, among them, **5** displays an interesting 2-fold interpenetrating 3D structure, in which intriguing 1D double helix chains are observed. In addition, the photoluminescent and magnetic properties of these samples are further investigated.

2. Experimental section

2.1. Materials and measurements

All starting chemicals were of reagent grade and used without further purification. Elemental analyses (C, H, N) were performed

* Corresponding author. Fax: +86 371 67766017.
E-mail addresses: yt.fan@zzu.edu.cn, yt.fan@371.net (Y.-T. Fan).

0022-4596/$ - see front matter © 2009 Published by Elsevier Inc.
doi:10.1016/j.jssc.2009.07.018

on a Carlo-Erba 1160 Elemental Analyzer. IR spectra were recorded in the region of 4000–400 cm^{-1} on a Nicolet NEXUS 470-FTIR Spectrophotometer with pressed KBr pellets. ^1H NMR spectra were determined at room temperature on Bruker DPX 400 Spectrometer. Excitation and emission spectra were obtained on an F-4500 HITACHI Fluorescence Spectrophotometer. Variable-temperature magnetic susceptibility data were obtained on a SQUID Susceptometer (Quantum Design, MPMS-5) in the temperature range of 5.0–300 K with an applied field of 500*G*. The diamagnetic contributions of the samples were corrected by using Pascal's constants [21].

The (1,3,4-thiadiazole-2,5-diyldithio)diacetic acid (H_2tzda) was prepared according to the literature method [22]. Elemental Anal. Cacld (%) for $C_6H_6N_2O_4S_3$: C, 27.07; H, 2.26; N, 10.53. Found: C, 27.12; H, 2.18; N, 10.19. IR data (cm^{-1}): 3082(m), 2983(m), 2927(m), 1735(s), 1712(s), 1384(s), 1364(m), 1299(m), 1202(s), 1182(s), 1050(s), 893(m), 780(m), 649(w). ^1H NMR (300 MHz, DMSO, 25 °C): $\delta = 13.0479$ (s, 2H, COOH), 4.1414(s, 4H, CH_2).

2.2. Synthesis of {[M(tzda)(bpe)] H_2O}$_n$ [M = Zn(**1**), Cd(**2**), Mn(**3**), Co(**4**)]

A mixture of $M(NO_3)_2 \cdot 6H_2O$ (0.4 mmol, M = Zn, 119 mg; M = Co, 116 mg) or $MnCl_2 \cdot 4H_2O$ (80 mg), or $Cd(NO_3)_2 \cdot 4H_2O$ (0.4 mmol, 123 mg), H_2tzda (0.4 mmol, 106 mg), NaOH (0.8 mmol, 32 mg), bpe (0.4 mmol, 74 mg) and deionized water (15 mL) was sealed in a Teflon-lined stainless steel vessel (25 mL), and then heated at 120 °C for 6 days. After being cooled to room temperature, crystals of **1** (colorless, block-like), **2** (colorless, block-like), **3** (colorless, block-like) and **4** (pink, block-like) were collected by filtration, respectively. Yield: 33% (**1**), 30% (**2**), 36% (**3**) and 39% (**4**) (based on transition metal). Anal. Calcd (%) for **1** ($C_{18}H_{18}ZnN_4O_5S_3$): C, 40.61; H, 3.38; N, 10.53. Found: C, 40.75; H, 3.48; N, 10.49. Anal. Calcd (%) for **2** ($C_{18}H_{18}CdN_4O_5S_3$): C, 37.31; H, 3.11; N, 9.67. Found: C, 37.39; H, 3.23; N, 9.42. Anal. Calcd (%) for **3** ($C_{18}H_{18}MnN_4O_5S_3$): C, 41.42; H, 3.45; N, 10.74. Found: C, 41.54; H, 3.55; N, 10.63. Anal. Calcd (%) for **4** ($C_{18}H_{18}CoN_4O_5S_3$): C, 41.11; H, 3.43; N, 10.66. Found: C, 41.25; H, 3.60; N, 10.48. IR data (KBr, cm^{-1}) for **1**: 3458(s), 1617(s), 1577(s), 1426(m), 1401(s), 1386(s), 1229(m), 1174(w), 1070(m), 1051(m), 1022(m), 931(w), 901(w), 835(m), 777(w), 744(w), 689(m); for **2**: 3451(s), 1592(s), 1585(s), 1427(m), 1413(s), 1387(s), 1229(m), 1177(w), 1070(m), 1049(m), 1020(m), 931(w), 900(w), 833(m), 774(w), 742(w), 694(m); for **3**: 3531(s), 1589(s), 1576(s), 1426(m), 1409(s), 1394(s), 1233(m), 1173(w), 1070(m), 1051(m), 1017(m), 931(w), 902(w), 826(m), 773(w), 743(w), 686(m) for **4**: 3530(s), 1593(s), 1575(s), 1424(m), 1410(s), 1389(s), 1234(m), 1175(w), 1069(m), 1052(m), 1020(m), 934(w), 901(w), 827(m), 775(w), 743(w), 688(m).

2.3. Synthesis of [Ni_2(tzda)$_2$(bpe)$_2$(H_2O)]$_n$ (**5**)

A mixture of $Ni(NO_3)_2 \cdot 6H_2O$ (0.4 mmol, 116 mg), H_2tzda (0.4 mmol, 106 mg), NaOH (0.8 mmol, 32 mg), bpe (0.4 mmol, 74 mg) and deionized water (15 mL) was sealed in a Teflon-lined stainless steel vessel (25 mL), and then heated at 130 °C for 4 days. After being cooled to room temperature, blue block crystals of **5** were collected by filtration. Yield: 45% based on Ni. Anal. Calcd (%) for $C_{36}H_{34}Ni_2N_8O_9S_6$: C, 41.84; H, 3.29; N, 10.85. Found: C, 41.96; H, 3.42; N, 10.76. IR data (KBr, cm^{-1}): 3422(s), 1615(s), 1575(s), 1425(m), 1403(s), 1381(s), 1223(m), 1168(w), 1072(m), 1054(m), 1023(m), 909(w), 829(m), 776(w), 746(w), 686(m).

2.4. X-ray crystallographic studies

Single crystals of **1** (0.31 × 0.12 × 0.08 mm), of **2** (0.23 × 0.21 × 0.18 mm), of **3** (0.44 × 0.38 × 0.21 mm), of **4** (0.22 × 0.15 × 0.11 mm), of **5** (0.17 × 0.08 × 0.03 mm) were selected for indexing and intensity data collection. The intensity data for **1–5** were collected at 291(2)–296(2) K on a Bruker Smart CCD diffractometer equipped with graphite-monochromatized Mo-$K\alpha$ (λ = 0.71073 Å).

All of the structures were solved by direct methods and expanded using Fourier techniques. The non-hydrogen atoms were refined with anisotropic thermal parameters. Hydrogen atoms were located at calculated positions and refined isotropically. The final cycle of full-matrix least squares refinement was based on the observed reflections and variable parameters. All calculations were performed using the SHELXL crystallographic software package [23]. Crystallographic data and structural refinements are summarized in Table 1. Selected bond distances and angles are listed in Table 2.

Table 1
Crystallographic data and structure refinement parameters for **1–5**.

Compounds	1	2	3	4	5
Empirical formula	$C_{18}H_{18}ZnN_4O_5S_3$	$C_{18}H_{18}CdN_4O_5S_3$	$C_{18}H_{18}MnN_4O_5S_3$	$C_{18}H_{18}CoN_4O_5S_3$	$C_{36}H_{34}Ni_2N_8O_9S_6$
Formula weight	531.91	578.94	521.48	525.47	1032.49
Crystal system	Triclinic	Triclinic	Triclinic	Triclinic	Monoclinic
Space group	$P\bar{1}$	$P\bar{1}$	$P\bar{1}$	$P\bar{1}$	*Pc*
a (Å)	9.0346(11)	9.2880(13)	9.3534(9)	9.3237(8)	8.5255(19)
b (Å)	11.3453(14)	10.9612(15)	10.4248(11)	10.2948(9)	9.781(2)
c (Å)	11.3835(13)	11.3631(15)	11.4927(12)	11.4186(9)	25.403(6)
α (deg)	73.1210(10)	77.508(2)	101.2930(10)	102.1470(10)	90
β (deg)	87.9230(10)	87.054(2)	92.0150(10)	91.8110(10)	90.394(4)
γ (deg)	75.9530(10)	77.559(2)	101.8410(10)	101.5620(10)	90
V (Å)	1082.4(2)	1102.9(3)	1072.22(19)	1046.62(15)	2118.3(8)
Z	2	2	2	2	2
μ (mm^{-1})	1.462	1.312	0.947	1.159	1.248
D_c ($g\,cm^{-3}$)	1.632	1.743	1.615	1.667	1.619
F(000)	544	580	534	538	1060
GOF on F^2	1.038	1.054	1.039	1.036	1.051
R_1, wR_2 ($I>2\sigma(I)$)	0.0358, 0.0755	0.0330, 0.0833	0.0275, 0.0681	0.0329, 0.0720	0.0906, 0.2268
R_1, wR_2 (all data)	0.0525, 0.0827	0.0396, 0.0888	0.0301, 0.0702	0.0420, 0.0778	0.1235, 0.2476
$\Delta\rho_{max}$, $\Delta\rho_{min}$ ($e\,Å^{-3}$)	0.295, −0.306	1.091, −0.567	0.378, −0.432	0.235, −0.313	1.099, −1.045

$R_1 = \sum||F_o|-|F_c||/\sum|F_o|$; $wR_2 = [\sum w(F_o^2-F_c^2)^2/\sum w(F_o^2)^2]^{1/2}$.

Table 2
Selected bond lengths (Å) and angles (deg) for **1–5**.

Compound **1**					
Zn(1)–O(3)#1	2.0303(17)	Zn(1)–O(4)#2	2.0452(17)	Zn(1)–O(1)	2.094(2)
Zn(1)–N(4)#3	2.1390(19)	Zn(1)–N(3)	2.1476(19)		
O(3)#1–Zn(1)–O(4)#2	125.41(8)	O(3)#1–Zn(1)–O(1)	89.33(8)	O(4)#2–Zn(1)–O(1)	145.26(8)
O(3)#1–Zn(1)–N(4)#3	90.78(8)	O(4)#2–Zn(1)–N(4)#3	85.12(7)	O(1)–Zn(1)–N(4)#3	96.05(8)
O(3)#1–Zn(1)–N(3)	97.57(7)	O(4)#2–Zn(1)–N(3)	85.82(7)	O(1)–Zn(1)–N(3)	89.23(8)
N(4)#3–Zn(1)–N(3)	170.18(8)				
Compound **2**					
Cd(1)–O(4)#1	2.2500(15)	Cd(1)–O(3)#2	2.2612(18)	Cd(1)–N(4)#3	2.3191(14)
Cd(1)–N(3)	2.3284(15)	Cd(1)–O(2)	2.4110(16)	Cd(1)–O(1)	2.4158(16)
O(4)#1–Cd(1)–O(3)#2	130.57(6)	O(4)#1–Cd(1)–N(4)#3	84.68(6)	O(3)#2–Cd(1)–N(4)#3	87.98(6)
O(4)#1–Cd(1)–N(3)	86.45(6)	O(3)#2–Cd(1)–N(3)	96.69(6)	N(4)#3–Cd(1)–N(3)	171.01(5)
O(4)#1–Cd(1)–O(2)	93.91(6)	O(3)#2–Cd(1)–O(2)	134.39(6)	N(4)#3–Cd(1)–O(2)	86.59(5)
N(3)–Cd(1)–O(2)	95.50(6)	O(4)#1–Cd(1)–O(1)	145.90(7)	O(3)#2–Cd(1)–O(1)	83.33(6)
N(4)#3–Cd(1)–O(1)	102.58(5)	N(3)–Cd(1)–O(1)	85.64(5)	O(2)–Cd(1)–O(1)	54.05(5)
Compound **3**					
Mn(1)–O(3)#1	2.0841(14)	Mn(1)–O(4)#2	2.1244(14)	Mn(1)–O(2)	2.2280(13)
Mn(1)–N(3)	2.2778(15)	Mn(1)–N(4)#3	2.2894(14)	Mn(1)–O(1)	2.3872(16)
O(3)#1–Mn(1)–O(4)#2	109.70(6)	O(3)#1–Mn(1)–O(2)	150.31(6)	O(4)#2–Mn(1)–O(2)	99.19(5)
O(3)#1–Mn(1)–N(3)	94.74(6)	O(4)#2–Mn(1)–N(3)	90.04(6)	O(2)–Mn(1)–N(3)	91.83(5)
O(3)#1–Mn(1)–N(4)#3	88.02(6)	O(4)#2–Mn(1)–N(4)#3	90.78(5)	O(2)–Mn(1)–N(4)#3	84.86(5)
N(3)–Mn(1)–N(4)#3	176.68(6)	O(3)#1–Mn(1)–O(1)	95.04(6)	O(4)#2–Mn(1)–O(1)	155.09(5)
O(2)–Mn(1)–O(1)	56.73(5)	N(3)–Mn(1)–O(1)	84.92(5)	N(4)#3–Mn(1)–O(1)	92.99(5)
Compound **4**					
Co(1)–O(3)#1	2.0132(18)	Co(1)–O(4)#2	2.0426(18)	Co(1)–O(2)	2.1570(18)
Co(1)–N(3)	2.156(2)	Co(1)–N(4)#3	2.1655(19)	Co(1)–O(1)	2.266(2)
O(3)#1–Co(1)–O(4)#2	107.85(8)	O(3)#1–Co(1)–O(2)	152.93(8)	O(4)#2–Co(1)–O(2)	98.45(7)
O(3)#1–Co(1)–N(3)	93.61(8)	O(4)#2–Co(1)–N(3)	90.22(8)	N(3)–Co(1)–O(2)	92.56(7)
O(3)#1–Co(1)–N(4)#3	88.57(8)	O(4)#2–Co(1)–N(4)#3	90.53(8)	O(2)–Co(1)–N(4)#3	84.83(7)
N(3)–Co(1)–N(4)#3	177.36(8)	O(3)#1–Co(1)–O(1)	94.76(8)	O(4)#2–Co(1)–O(1)	157.34(7)
O(2)–Co(1)–O(1)	59.31(7)	N(3)–Co(1)–O(1)	86.79(8)	N(4)#3–Co(1)–O(1)	91.55(7)
Compound **5**					
Ni(1)–O(5)	2.031(11)	Ni(1)–O(4)#1	2.064(10)	Ni(1)–O(2)	2.070(10)
Ni(1)–N(8)#2	2.106(12)	Ni(1)–O(9)	2.137(10)	Ni(1)–N(5)	2.139(13)
Ni(2)–O(6)	2.032(10)	Ni(2)–O(1)	2.055(11)	Ni(2)–N(7)	2.084(12)
Ni(2)–O(8)#3	2.084(13)	Ni(2)–N(6)#4	2.097(12)	Ni(2)–O(9)	2.123(10)
O(5)–Ni(1)–O(4)#1	90.3(5)	O(5)–Ni(1)–O(2)	94.1(5)	O(4)#1–Ni(1)–O(2)	174.5(4)
O(5)–Ni(1)–N(8)#2	86.0(5)	O(4)#1–Ni(1)–N(8)#2	89.4(5)	O(2)–Ni(1)–N(8)#2	87.6(5)
O(5)–Ni(1)–O(9)	89.4(4)	O(4)#1–Ni(1)–O(9)	89.8(4)	O(2)–Ni(1)–O(9)	93.6(4)
N(8)#2–Ni(1)–O(9)	175.3(5)	O(5)–Ni(1)–N(5)	177.0(5)	O(4)#1–Ni(1)–N(5)	86.7(5)
O(2)–Ni(1)–N(5)	88.8(4)	N(8)#2–Ni(1)–N(5)	94.0(5)	O(9)–Ni(1)–N(5)	90.6(4)
O(6)–Ni(2)–O(1)	93.5(5)	O(6)–Ni(2)–N(7)	92.7(5)	O(1)–Ni(2)–N(7)	173.7(5)
O(6)–Ni(2)–O(8)#3	174.7(4)	O(1)–Ni(2)–O(8)#3	87.2(5)	N(7)–Ni(2)–O(8)#3	86.5(5)
O(6)–Ni(2)–N(6)#4	88.2(4)	O(1)–Ni(2)–N(6)#4	85.1(4)	N(7)–Ni(2)–N(6)#4	93.9(5)
O(8)#3–Ni(2)–N(6)#4	86.7(4)	O(6)–Ni(2)–O(9)	97.9(4)	O(1)–Ni(2)–O(9)	86.5(4)
N(7)–Ni(2)–O(9)	93.8(4)	O(8)#3–Ni(2)–O(9)	87.4(4)	N(6)#4–Ni(2)–O(9)	170.0(4)

Symmetry transformations used to generate equivalent atoms: For **1**: #1*x*, *y*, *z*+1; #2−*x*+1, −*y*+2, −*z*+1; #3*x*, *y*+1, *z*−1. For **2**: #1−*x*+1, −*y*+2, −*z*+1; #2*x*, *y*, *z*+1; #3*x*, *y*+1, *z*−1. For **3**: #1*x*, *y*, *z*−1; #2−*x*+1, −*y*+1, −*z*+1; #3*x*, *y*+1, *z*+1. For **4**: #1*x*, y, *z*−1; #2−*x*+2, −*y*+1, −*z*+1; #3*x*, *y*+1, *z*+1. For **5**: #1: *x*, *y*+1, *z*; #2: *x*−1, −*y*+1, *z*+1/2; #3: *x*, *y*−1, *z*; #4: *x*−1,−*y*, *z*−1/2.

3. Results and discussion

3.1. Description of the crystal structures

3.1.1. Crystal structures of *1* and *2*

Single-crystal X-ray diffraction analyses reveal that compounds **1** and **2** crystallize in the triclinic crystal system with space group $p\bar{1}$ and display a 2D bilayered structure generated by $[M(\text{tzda})]_n$ [M = Zn (**1**), Cd(**2**)] double chain motif linking bpe spacers. The asymmetric units in **1** and **2** all contain one metal atom, one tzda ligand, one bpe molecule and one free water molecule. However, the coordination environment of central metal atom in **1** is different from that in **2**. In **1**, each Zn(II) atom locates in a distorted trigonal bipyramidal coordination environment formed by three O atoms from three different tzda ligands occupying equatorial plane [Zn–O = 2.0303(17)–2.094(2) Å], and two bpe N atoms occupying the axial sites[Zn–N = 2.1476 (19)–2.1390(19) Å] (Fig. 1a). While in **2**, every Cd(II) atom exhibits a distorted octahedral geometry, composed of four carboxylic O atoms from three tzda anions [Cd– = 2.2500(15)–2.4158(16) Å] and two N atoms from two bpe ligands [Cd–N = 2.3191(14)–2.3284(15) Å] (Fig. 1b). These Zn–O/N and Cd–O/N distances fall in the normal range found in other Zn and Cd complexes [11,24–26].

In **1** and **2**, each tzda ligand adopts completely *trans*-configuration and acts as a μ_3-bridge to connect three metal atoms. The tzda ligand exhibits monodentate/*syn*,*syn*-bridging-bidentate mode in **1** and chelating-bidentate/*syn*,*syn*-bridging-bidentate mode in **2** through its two carboxylate groups, respectively. The transformation of coordination mode of tzda ligand from **1** to **2** is that the monodentate carboxylate group changes to bidentate chelating carboxylate group, and as a result, the Cd(II) atom in **2** is six-coordinated while Zn(II) atom in **1** is five-coordinated. Based on above connection modes, two metal atoms are bridged by a pair of carboxylate group ends from two different tzda anions into a dimeric M_2 unit [M = Zn (**1**), Cd(**2**)] and then these units are linked by tzda anions to form an extended 1D $[M(\text{tzda})]_n$ zigzag double chain along the *c*-axis (Fig. 1c). The $M\cdots M$ distances in the intrachain dimeric M_2 units are 3.963 Å (Zn⋯Zn) in **1** and 3.951 Å (Cd⋯Cd) in **2**, respectively.

Meanwhile, all bpe ligands adopt an *anti*-configuration and link adjacent double chains into a unique 2D bilayered network (Fig. 1d). This 2D bilayered network is can also be regarded as being constructed by two layers of [*M*(tzda)(bpe)] linked by μ_2-carboxylate groups of tzda anions. Two adjacent pyridyl rings between two layers, defined by N3, C7, C8, C9, C10, C11 and N4, C14, C15, C16, C17, C18, respectively, are basically parallel, only slightly twisted by 4.4° in **1** and 5.8° in **2**. The centroid–centroid distance and centroid-plane distance between the pyridyl rings are 4.063 and 3.567 Å in **1**, and 3.917 and 3.637 Å in **2**, respectively, indicating the existence of intralayered π–π stacking interactions [27]. Among neighboring 2D bilayered networks, nonbonding S2⋯S3 distances are 3.630 Å in **1** and 3.596 Å in **2**, which are less than the sum of the van der Waals' radii of two S atoms (3.74 Å) and indicates weak S⋯S interactions [28,29]. Furthermore, all lattice water molecules participate in the formation of two kinds of interlayered hydrogen-bonding [O5⋯O1a, 2.924(3) Å (a: –*x*+2, –*y*+1, –*z*+2); O5⋯S1, 3.570(3) Å] in **1** and only one sort of hydrogen bond is formed between lattice water molecules and carboxylate O atoms [O5⋯O1b, 2.922(3) Å (*b*: *x*–1, *y*, *z*–1)] in **2**. Thus, combining S⋯S interactions and hydrogen bonds, these 2D bilayered networks are extended into a 3D supramolecular framework (Fig. S1).

3.1.2. Crystal structures of **3** and **4**

Compounds **3** and **4** are isostructural and feature 2D bilayered networks as **1** and **2** do. Therefore, only the structure of **3** will be detailed by comparing with the structure of **2**. Each Mn(II) atom in **3** is six-coordinated in a distorted octahedral geometry, defined by four O atoms from three tzda anions in equatorial plane [Mn–O = 2.0841(14)–2.3872(16) Å] and two N atoms from two bpe ligands in the axial positions [Mn–N = 2.2778(15) –2.2894(14) Å], which is similar to the coordination environment of Cd (II) atoms in **2**.

Like that in **2**, the tzda ligand adopts the chelating-bidentate/bridging-bidentate mode, bridging Mn(II) atoms to form 1D infinite $[Mn(tzda)]_n$ double chains. These 1D chains are further connected by *anti*-bpe ligands, leading to an infinite 2D bilayered structure (Fig. 2). It is noteworthy that intralayered π–π stacking in **3** occurs between two neighboring pyridyl rings both defined by N3, C7, C8, C9, C10, and C11, since the pyridyl rings are parallel and separated by a plane–plane distance of 3.565 Å and a centroid–centroid distance of 4.432 Å [27]; while no intralayered π–π interaction exists between two pyridyl rings defined by N3, C7, C8, C9, C10, C11 and N4, C14, C15, C16, C17, C18, due to the dihedral angle of 75.4°. This is the significant difference between the structures of **3** and **2**, and which arises from the flexible nature of bpe ligand. In **3**, weak interlayered S⋯S interactions also occur with distance of 3.634 Å ($S_2 \cdots S_3$), just as they do in **2**. However, different from those in **2**, there are two types of hydrogen bonds formed by the lattice water molecules with carboxylate O atoms [O5⋯O1a, 2.915(2) Å (*a*: –*x*+1, –*y*+1, –*z*)] or thiadiazole N atoms [O5⋯N2b(*b*: –*x*+1, –*y*+1, –*z*+1), 3.100(3) Å] in **3**. Depending on these S⋯S interactions and hydrogen bonds, a final 3D supramolecular network produces from 2D layered networks.

3.1.3. Crystal structure of **5**

Single crystal structure analysis reveals that compound **5** crystallizes in the monoclinic space group *Pc* and is a 2-fold interpenetrating three-dimensional polymer comprising $[Ni_2(OCO)_2(H_2O)]_n$ binuclear units bridged by tzda and bpe. The asymmetric unit of **5** contains two crystallographically independent Ni(II) atoms, two tzda ligands, two bpe molecules and one coordinated water molecule. As illustrated in Fig. 3a. Ni1 and Ni2 are both six-coordinated in a significantly contorted $[NiN_2O_4]$ octahedral coordination sphere formed by one oxygen atom from tzda ligand, two nitrogen atom from different bpe, one water molecule occupying the basal plane, and two oxygen atoms from another two tzda ligands occupying the axial sites. The Ni–N distances range between 2.084(12) and 2.139(13) Å, and the Ni–O bonds range between 2.031(11) and 2.137(10) Å, being comparable to reported values [30]. The axial O2–Ni1–O4A (*x*, *y*+1, *z*) and O6–Ni2–O8A (*x*, *y*–1, *z*) angles are 174.5(4)° and 174.7(4)°, respectively.

Two kinds of tzda both display *trans*-configuration and serves as triconnector (μ_3) linking three metal centers; one carboxylate group bidentately bridges two Ni atoms in *syn*–*syn* fashion, and the other one coordinates to one Ni atom in monodentate fashion, as they do in **1**. In **5**, two Ni atoms (Ni1 and Ni2) are joined by a pair of *syn*,*syn*-bridging carboxylate groups and one water molecule to form a $[Ni1Ni2(OCO)_2O]$ dinickel unit. Along the *b* axis, these dinickel units are bridged by tzda anions to generate an infinite 1D ladder chain (Fig. 3b). The Ni1⋯Ni2 distances in the dinuclear units are 3.596 °Å, while the Ni1⋯Ni1 and Ni2⋯Ni2 separations across a pair of tzda ligands are the same, being 9.781 Å.

Two types of pillared bpe ligands are also observed in **5**. Both of them adopt *anti*-conformation and two pyridine rings in different bpe ligands are almost coplanar with the dihedral angle of 6.7° and 5.8°, respectively. Noticeably, along the direction of *b* axis, two types of bpe bridge $[Ni1Ni2(OCO)_2O]$ dinickel units to form a left-handed (Fig. 3c) or right-handed double helix-chain structures. And in each single helical chain of double helix chains, four $[Ni1Ni2(OCO)_2O(bpe)]$ units complete one helical turn with a pitch of 19.562 Å. Whereafter, a pair of single helical chains are connected by tzda ligands through Ni_2(II) nodes along the *b* axis, forming a large 1D square grid-like channel (13.554×13.465 Å^2 based on d_{Ni-Ni}). These channels are transferred to the neighboring channels with opposite helical orientation through Ni_2(II) nodes, leading to the formation of a racemic 3D framework which includes equal amounts of left- and right-handed helices (Fig. 3d). This 3D framework is significantly different from that of reported $[Ni(tzda)(4,4'\text{-bipy})(H_2O)]_n$ [19], formed by Ni-tzda 2D layers linking rigid 4,4′-bipy ligands. It should be emphasized that longer and flexible bpe ligands have resulted in the formation of large square grid-like channel in the 3D framework, revealing that the second ligand has a great influence on the structures of coordination polymers. However, due to the absence of large guest molecules to fill the void channel during the assembly process, the potential voids are filled *via* mutual interpenetration of another independent framework, generating the final 2-fold interpenetrating three-dimensional architecture (Fig. 3e). Additionally, all coordinated water molecules participate in forming two sorts of intrachain O–H⋯O hydrogen bonds with uncoordinated carboxylate oxygen atoms of tzda ligands [O9⋯O7a, 2.583(16) Å (*a*: *x*, *y*–1, *z*+1/2); O9⋯O3b, 2.676(16) Å (*e*: *x*, *y*+1, *z*)] and further stabilize the 3D network of **5**.

It is obvious from the above structural description of **1–5** that the second ligand flexible bpe has significant effect on the final structures of the resulting complexes. Comparisons of the structures of **1**, **4** and **5** with previously studied 1D chains of transition metal coordination polymers $[M(tzda)(H_2O)_4]_n$ [*M* = Zn, Co and Ni] formed by bis-monodentate tzda ligand bridging two metal ions [19] suggest the second ligand bpe causes the distinctness of the coordination modes of tzda ligands and finally results in the formation of different structures. In addition, the length and flexibility of the second ligand have significant effect on the structures, as evidenced by two facts, one is that **5** displays a 2-fold interpenetrated 3D network, while no interpenetration appears in metal-tzda-bipy polymers due to the short 4,4′-bipy pillar ligands [19]; the other is that crystal packing structures of **2**

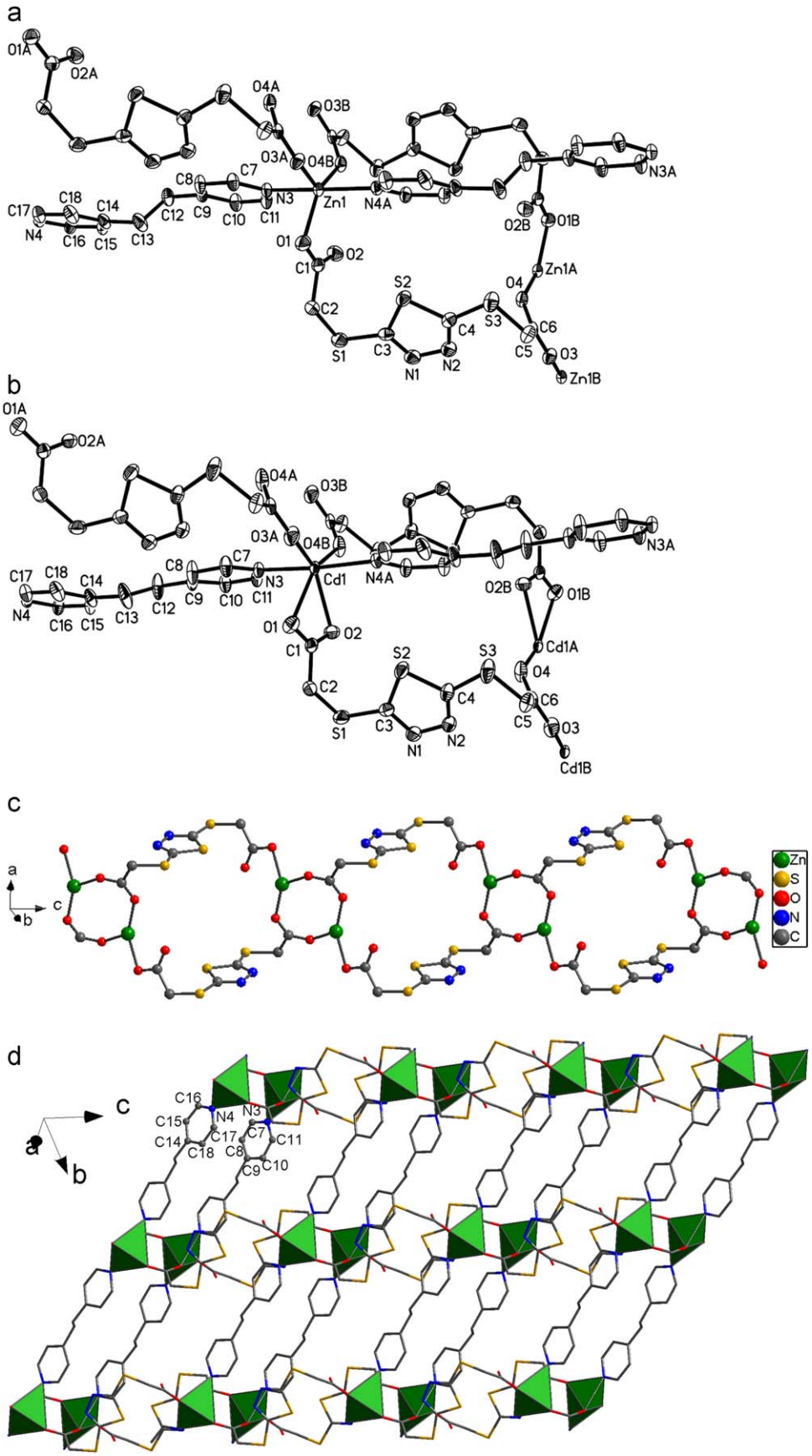

Fig. 1. (a) Perspective view showing coordination environment of Zn and the bridging mode of tzda in **1**. Hydrogen atoms are omitted for clarity. (b) Perspective view showing coordination environment of Cd and the bridging mode of tzda in **2**. Hydrogen atoms are omitted for clarity. (c) Double chain structure constructed from Zn atoms and tzda ligands in **1**. (d) 2D double-layer structure of **1**.

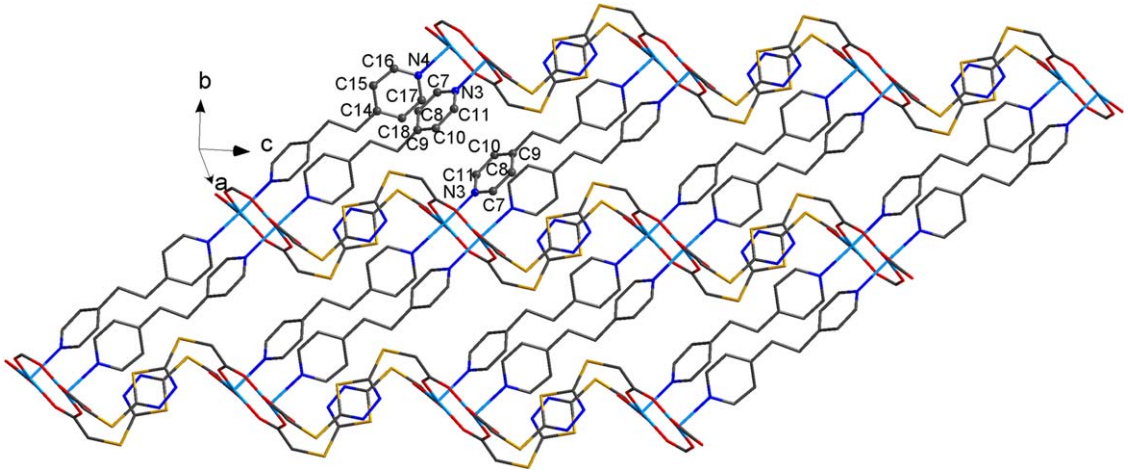

Fig. 2. 2D double-layer structure of **3**.

and **3** are different, even though they have similar cell parameters (Table 1) and display similar 2D-layed structure. These results demonstrate that the structures of entangled metal-tzda system can be modulated by incorporation of the secondary ligands.

3.2. Infrared spectra and photoluminescent properties

The IR spectra of the five compounds display the characteristic absorptions of tzda anion. The disappearance of the band at about 1710–1740 cm^{-1} assigned to the stretching bands of –COOH indicates complete deprotonation of the carboxyl groups. The strong bands at 1617, 1577 and 1401, 1386 cm^{-1} for **1**, 1592, 1585 and 1413, 1390 cm^{-1} for **2**, 1589, 1576 and 1409, 1391 cm^{-1} for **3**, 1596, 1575 and 1410, 1389 cm^{-1} for **4**, and 1615, 1575 and 1403, 1381 cm^{-1} for **5** are assigned to the asymmetric and symmetric stretching bands of COO^- groups, respectively, suggesting that the COO^- groups function in different coordination modes [31]. Compounds **1–5** also show broad –OH stretching bands in the region of 3422–3531 cm^{-1}, indicating the presence of water molecules in these compounds. Furthermore, the characteristic IR bands of the thiadiazole ring due to vibrations of thiadiazole ring appear at about 1049–1054 cm^{-1} [32,33] and these bands almost have the same features as they do in the free ligand, suggesting that the thiadiazole ring keeps free of coordination in five compounds. All these spectroscopic features of **1–5** are in good agreement with the corresponding crystal structures and charge balance considerations.

Inorganic–organic hybrid coordination polymers with d^{10} metal centers have been found to exhibit photoluminescence properties and have potential applications in optoelectronic devices [34,35]. Thus the luminescent behaviors of compounds **1** and **2** are investigated in the solid state at room temperature, and the results are provided in Fig. 4. Compound **1** shows one weak emission band at about 367 nm and one intense peak at 498 nm when exited at 315 nm, while **2** exhibits one intense and one weak shoulder peaks at about 369 and 459 nm exited at 320 nm, respectively. Since free ligand H_2tzda displays an emission band at ca. 375 nm upon photoexciation at 315 nm, the emissions 367 nm for **1** and 369 nm for **2** should be ascribed to intraligand fluorescence emission. It is obvious that the locations of emission peaks at 498 nm for **1** and 459 nm for **2** are different from that of H_2tzda ligand, and accordingly these peaks may be assigned to ligand-to-metal charge transfer (LMCT) [36]. The different emission peaks of **1** and **2** are probably due to the differences of central metal ions and coordination environment around them, because photoluminescence behavior is closely associated with the metal ions and the ligands coordinated around them [37].

3.3. Magnetic properties

The magnetic susceptibility measurements of compounds **3**, **4** and **5** were carried out over the temperature range 5–300 K. The magnetic behavior of **3** is illustrated in Fig. 5 by means of plots of $\chi_M T'$ and χ_M versus the temperature. At 300 K, the value of $\chi_M T'$ is 9.24 $cm^3\,mol^{-1}\,K^{-1}$ and the magnetic moment value is 8.59 μ_B, which is somewhat higher than expected for two uncoupled high spin Mn(II) ions (8.36 μ_B, S = 5/2) [38]. As the temperature is lowered, the $\chi_M T'$ value continuously decreases and reaches a minimum 3.286 $cm^3\,mol^{-1}\,K$ at 5 K^{-1}, which indicates the occurrence of an antiferromagnetic interaction between the bridged Mn(II) ions. Since the 2D structure of **3** is constructed by longer bpe and $–CH_2SC_2N_2SSCH_2–$ spacers bridging binuclear building units $[Mn_2(OCO)_2]$, it is reasonable to analyze the magnetic susceptibility data presuming **3** to be a binuclear Mn(II) complex from a magnetic point of view. Assuming isotropic exchange, Eq. (1) for the magnetic susceptibility per Mn(II) for the dinuclear Mn(II) system is induced from the Hamiltonian $H = -2JS_1 \cdot S_2$ with $S_1 = S_2 = 5/2$ [21,39,40]:

$$\chi_M = \frac{2N\beta^2 g^2}{kT}\left[\frac{55 + 30x^{10} + 14x^{18} + 5x^{24} + x^{28}}{11 + 9x^{10} + 7x^{18} + 5x^{24} + 3x^{28} + x^{30}}\right] \quad (1)$$

where $x = \exp(-J/kT)$; J is the exchange coupling constant for binuclear Mn(II) ions.

The least-square analysis of magnetic susceptibilities data gave the following set of parameters: $J = -1.054\ cm^{-1}$, $g = 2.14$ with the agreement factor $R = \sum[(\chi_M)_{exp}-(\chi_M)_{cacl}]^2/\sum[(\chi_M)_{exp}]^2 = 2.86 \times 10^{-5}$. The J value suggests that a weak antiferromagnetic interaction between Mn(II) ions mediated through the double *syn–syn* mode μ_2-carboxyl bridges. Since *syn–syn* carboxyl bridges can provide a small metal–metal distance and result in a good overlap of the magnetic orbitals, an antiferromagnetic coupling is always induced [41]. The magnetic property of **3** is quite comparable to those reported for other Mn(II) species with similar double carboxyl bridges [42,43].

The χ_M versus T plot and $\chi_M T'$ versus T plot for **4** are shown in Fig. 6. The value of $\chi_M T'$ starts 3.91 $cm^3\,mol^{-1}\,K^{-1}$ at 300 K, which is close to that expected for an isolated binuclear Co(II) ions (3.75 $cm^3\,mol^{-1}\,K$ for $g_{av} = 2$) at room temperature [44]. The $\chi_M T'$ value continuously decreases and reaches a minimum

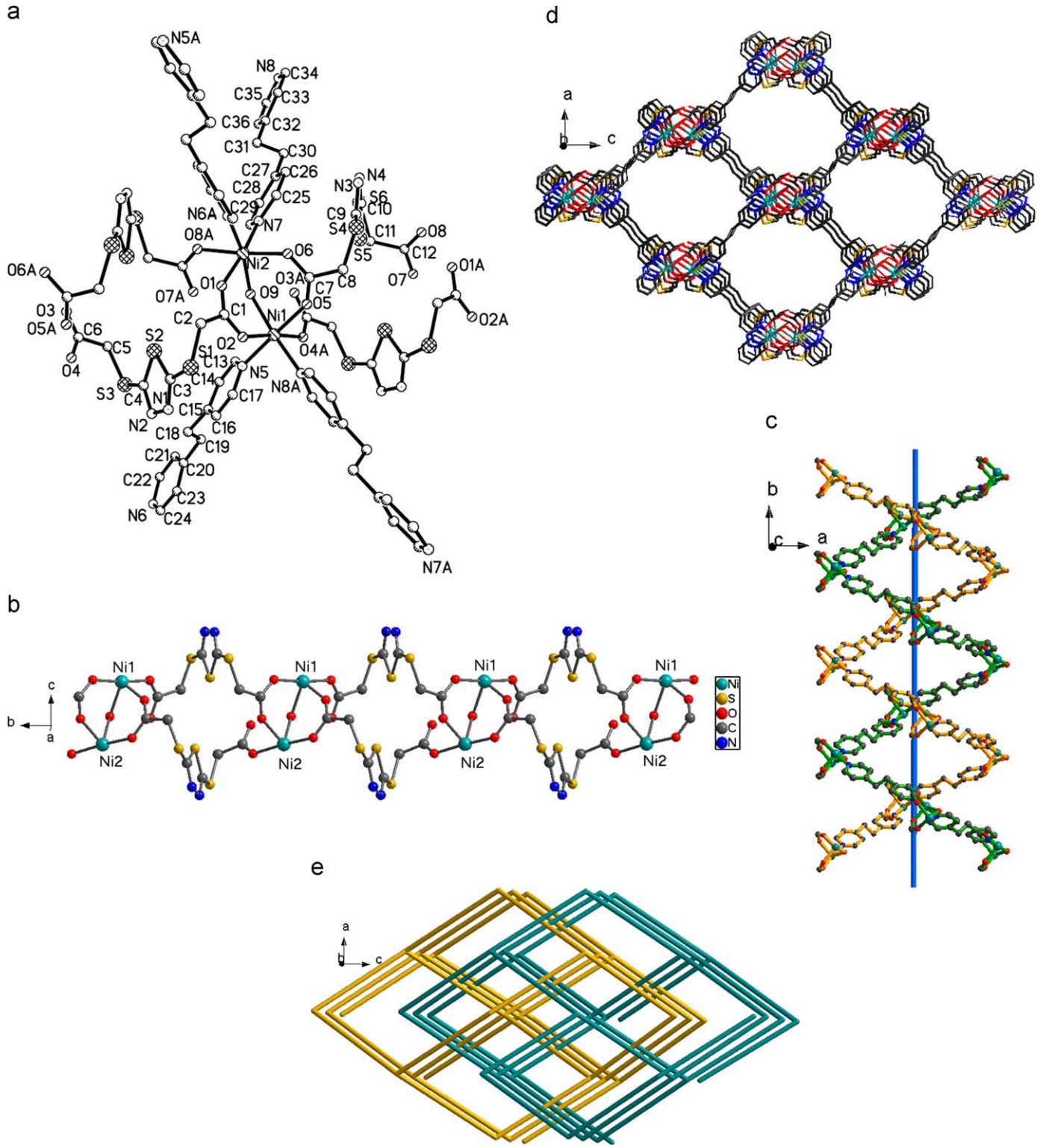

Fig. 3. (a) Perspective view showing coordination environment of Ni and the bridging mode of tzda in **5**. Hydrogen atoms are omitted for clarity. (b) 1D ladder-chain structure constructed by dinuclear Ni_2 units and tzda in **5**. (c) Double helix chains constructed by dinuclear Ni_2 units and bpe in **5**. (d) 3D framework of **5** with square grid-like channel viewing along *b* axis. (e) Schematic representation of 2-fold interpenetrating 3D network of **5** (each node represents a dinuclear Ni_2 unit).

1.02 $cm^3\ mol^{-1}$ K at 5 K, implying the antiferromagnetic exchange between the bridged Co(II) ions. Since the 2D structure of **4** is same as that of **3**, the magnetic susceptibility data are fitted assuming that **4** is also a binuclear complex as **3** is. Thus, Eq. (2) is used to fit the experimental susceptibility data, in which the effective spin of binuclear unit is treated as a classic spin, and the binuclear magnetic susceptibility $\chi_{M(Co-Co)}$ is based on Heisenberg binuclear model ($H = -2JS_1 \cdot S_2$, $S_1 = S_2 = 3/2$) [44]:

$$\chi_M = \frac{2N\beta^2 g^2}{kT}\left[\frac{14 + 5x^6 + x^{10}}{7 + 5x^6 + 3x^{10} + x^{12}}\right] \quad (2)$$

where $x = \exp(-J/kT)$.

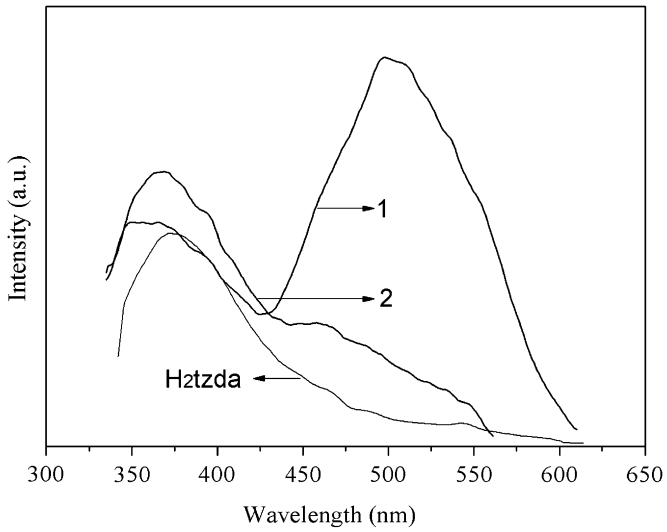

Fig. 4. Solid-state emission spectra of **1**, **2** and H_2tzda at room temperature.

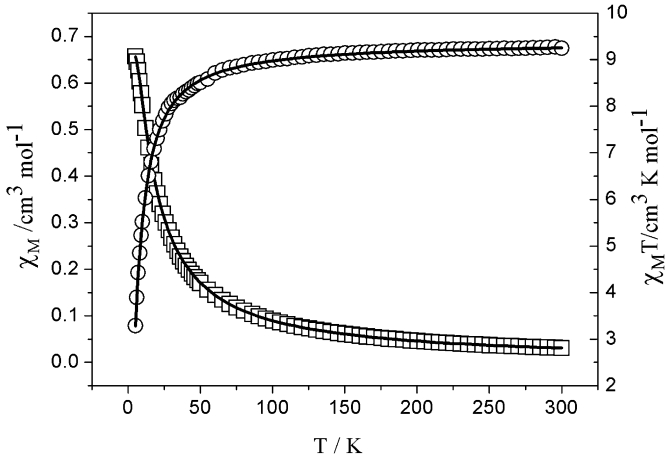

Fig. 5. The χ_M and $\chi_M T'$ vs T plots for **3** with solid lines for the best fit.

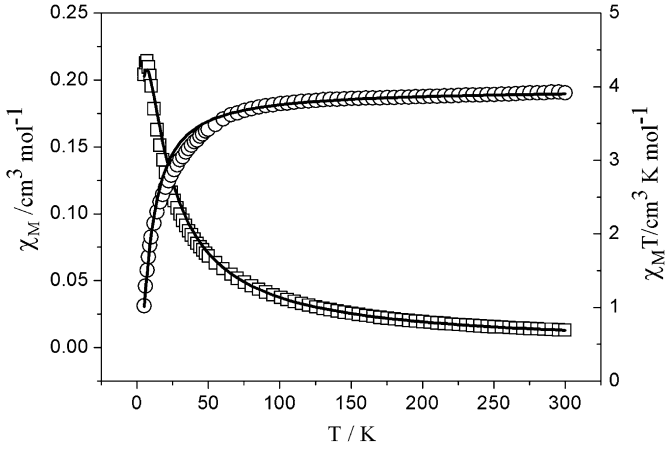

Fig. 6. The χ_M and $\chi_M T'$ vs T plots for **4** with solid lines for the best fit.

The best parameters obtained by a standard least squares fitting are $J = -1.53\,cm^{-1}$, $g = 2.05$, and $R = 2.7 \times 10^{-3}$. The value of J demonstrates that a weak antiferromagnetic coupling exists between the Co(II) ions which is the result of the double *syn–syn* carboxyl bridges.

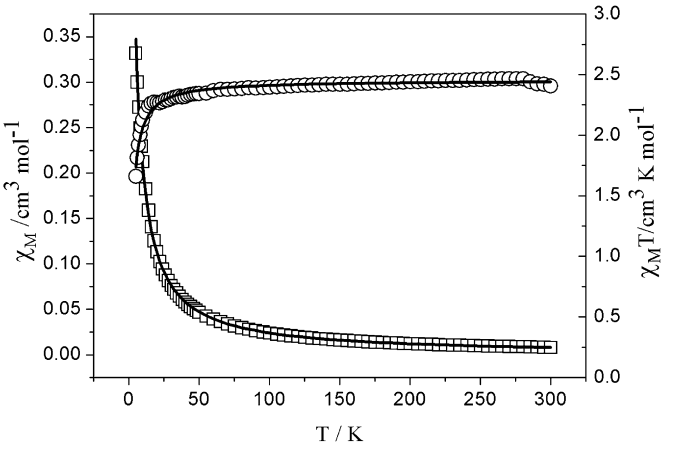

Fig. 7. The χ_M and $\chi_M T'$ vs T plots for **5** with solid lines for the best fit.

Fig. 7 gives the $\chi_M T'$ versus T and χ_M^{-1} versus T curves for **5**. At room temperature, the $\chi_M T'$ value is $2.40\,cm^3\,mol^{-1}\,K$ and somewhat higher than that ($2.0\,cm^3\,mol^{-1}\,K$) expected for two magnetically isolated spin-only Ni(II) ions, indicating that the orbital contribution is incompletely quenched [45]. Upon cooling, the $\chi_M T'$ value slightly decreases until 18 K and below 18 K, the $\chi_M T'$ value rapidly decreases on further cooling; while the χ_M increases gradually to $0.332\,cm^3\,mol^{-1}$ at 5 K. The general features of two curves (χ_M and $\chi_M T'$) are characteristic of intramolecular antiferromagnetic coupling between nickel ions, which has been observed in the reported compounds [Ni(pdc)(4,4′-bipy)]·1/2MeOH(H_2pdc = Pyridine-2,6-dicarboxylic acid) [46] and [Ni(tzda)(4,4′-bipy)(H_2O)]$_n$ [21]. Similar to those of **3** and **4**, the 3D structure of **5** is assembled by long bpe and $-CH_2SC_2N_2SSCH_2-$ spacers bridging binuclear [$Ni_2(OCO)_2O$] building units, and thus **5** can also be considered as binuclear system from a magnetic point of view. A reported empirical formula for analyzing binuclear Ni(II) system is used to fit magnetic susceptibility data [47]:

$$\chi_M = \frac{N\beta^2 g^2}{kT}\left[\frac{2\exp x + 10\exp 3x}{1 + 3\exp x + 5\exp 3x}\right], \text{ where } x = J/kT. \quad (3)$$

Using this method, the best-fit parameters for **5** are $J = -0.34\,cm^{-1}$, $g = 2.19$, and $R = 6.79 \times 10^{-4}$. The J value again confirms the weak antiferromagnetic interaction between the bridged Ni(II) ions. Although the magnetic susceptibility data of **3**, **4** and **5** are all based on the binuclear model, different from those of compounds **3** and **4**, there are two pathways of magnetic interaction within the binuclear Ni(II) units from the structural point of view: the two carboxyl groups and one water bridge between two Ni(II) ions, thus small overlaps between the magnetic orbits of Ni(II) ions occurs, accounting for the weak antiferromagnetic coupling.

4. Conclusions

In summary, by changing metal ions and/or synthetic conditions, five new coordination polymers based on flexible mixed ligands of H_2tzda and bpe have been hydrothermally synthesized and characterized by X-ray diffraction, fluorescent emission spectra and low-temperature magnetic measurements, respectively. Compounds **1–4** exhibit 2D layer structures all formed from double-chain [M(tzda)]$_n$ [M = Zn(**1**), Cd(**2**), Mn(**3**), Co(**4**)]

structure linked by bpe ligands. The delicate structural differences among **1–4** should be attributed to the nature of metal coordination and the diverse conformations of ligands since same synthetic condition was used. 5 displays a novel 2-fold interpenetrated three-dimensional coordination network containing double helix chains and the formation of interpenetration and helix chain is mainly ascribed to the function of longer and flexible bpe space. This work suggests that the incorporation of bpe as auxiliary ligand in metal-tzda system contributes to construction of extended structures, and also indicates the structures of polymers can be manipulated by introducing the secondary ligands.

Supplementary material

Crystallographic data for the five structures reported in this paper have been deposited in Cambridge Crystallographic Data Center as supplementary publication, CCDC nos. 624100, 624099, 624101, 722761, and 722762 for **1**–**5**, respectively. The data can be obtained free of charge on application to CCDC, 12 Union Road, Cambridge CB2 1EZ, UK (Fax: +44-1223-336-033; E-mail to: deposit@ccdc.cam.ac.uk). 3D supramolecular network of **1** (Fig. S1a) and 3D supramolecular network of **2** (Fig. S1b).

Acknowledgments

This work was sponsored by the Specialized Research Fund for the Doctoral Program of Higher Education (SRFDP, 20070459007), the National Natural Science Foundation of China (no. 20871106, 90610001), the Base and Cutting-edge Technology Research Project of Henan Province (092300410033), the Foundation for Young Backbone Teacher of Henan Colleges and Universities in 2008 (no. 198), the Natural Science Research Assistance Program from the Education Department of Henan Province (2009A150007, 2009A430024), and the Energy and Technology Program from Zhengzhou University.

Appendix A. Supplementary material

Supplementary data associated with this article can be found in the online version at doi:10.1016/j.jssc.2009.07.018.

References

[1] L. Carlucci, G. Ciani, D.M. Proserpio, Coord. Chem. Rev. 246 (2003) 247.
[2] S. Kitagawa, R. Kitaura, S. Noro, Angew. Chem. Int. Ed. 43 (2004) 2334.
[3] J.L.C. Rowsell, A.R. Millward, K.S. Park, O.M. Yaghi, J. Am. Chem. Soc. 126 (2004) 5666.
[4] J.L.C. Rowsell, E.C. Spencer, J. Eckert, J.A.K. Howard, O.M. Yaghi, Science 309 (2005) 1350.
[5] G. Férey, C. Mellot-Drazneiks, C. Serre, F. Millange, J. Dutour, S. Surblé, I. Margiolaki, Science 309 (2005) 2040.
[6] G. Tian, G.S. Zhu, X.Y. Yang, Q.R. Fang, M. Xue, J.Y. Sun, Y. Wei, S.L. Qiu, Chem. Commun. 25 (2005) 1396.
[7] N.L. Rosi, J. Eckert, M. Eddaoudi, D.T. Vodak, J. Kim, M. O'Keeffe, O.M. Yaghi, Science 300 (2003) 1127.
[8] O. Fabelo, J. Pasán, L. Cañdillas-Delgado, F.S. Delgado, A. Labrador, F. Lloret, M. Julve, C. Ruiz-Pérez, Cryst. Growth Des. 8 (2008) 3984.
[9] Y.Q. Wei, Y.F. Yu, K.C. Wu, Cryst. Growth Des. 8 (2008) 2087.
[10] H.F. Zhu, J. Fan, T.A. Okamura, Z.H. Zhang, G.X. Liu, K.B. Yu, W.Y. Sun, N. Ueyama, Inorg. Chem. 45 (2006) 3941.
[11] S.N. Wang, J.F. Bai, H. Xing, Y.Z. Li, Y. Song, Y. Pan, M. Scheer, X.Z. You, Cryst. Growth Des. 7 (2007) 747.
[12] L.F. Ma, L.Y. Wang, X.K. Huo, Y.Y. Wang, Y.T. Fan, J.G. Wang, S.H. Chen, Cryst. Growth Des. 8 (2008) 620.
[13] B. Chen, Y. Ji, M. Xue, F.R. Fronczek, E.J. Hurtado, J.U. Mondal, C. Liang, S. Dai, Inorg. Chem. 47 (2008) 5543.
[14] F.A. Almeida Paz, J. Klinowski, Inorg. Chem. 43 (2004) 3948.
[15] G.H. Wang, Z.G. Li, H.Q. Jia, N.H. Hu, J.W. Xu, Cryst. Growth Des. 8 (2008) 1932.
[16] F.M. Tabellion, S.R. Seidel, A.M. Arif, P.J. Stang, J. Am. Chem. Soc. 123 (2001) 7740.
[17] Y.Q. Lan, S.L. Li, Y.M. Fu, D.Y. Du, H.Y. Zang, K.Z. Shao, Z.M. Su, Q. Fu, Cryst. Growth Des. 9 (2009) 1353.
[18] D.K. Kumar, A. Das, P. Dastidar, Cryst. Growth Des. 6 (2006) 1903.
[19] Y.T. Wang, X.Q. Shen, Y.T. Fan, H.C. Yao, H.W. Hou, Supramol. Chem. 20 (2008) 501.
[20] Y.T. Wang, L.P. Zhang, Y.T. Fan, H.W. Hou, X.Q. Shen, Inorg. Chim. Acta 360 (2007) 2958.
[21] O. Kahn, Molecular Magnetism, VCH Publisher, New York, 1993.
[22] X.H. Lou, Y. Zhu, H. Gao, A.X. Zhu, Y.T. Fan, H.W. Hou, H.J. Lu, Chin. J. Inorg. Chem. 21 (2005) 716.
[23] G.M. Sheldrick, SHELXL-97 Program for the Solution and Refinement of Crystal Structures, University of Göttingen, Germany, 1997.
[24] L.L. Wen, D.B. Dang, C.Y. Duan, Y.Z. Li, Z.F. Tian, Q.J. Meng, Inorg. Chem. 44 (2005) 7161.
[25] J.J. Wang, L. Gou, H.M. Hu, Z.X. Han, D.S. Li, G.L. Xue, M.L. Yang, Q.Z. Shi, Cryst. Growth Des. 7 (2007) 1514.
[26] G.X. Liu, Y.Q. Huang, Q. Chu, T. Okamura, W.Y. Sun, H. Liang, N. Ueyam, Cryst. Growth Des. 8 (2008) 3233.
[27] C. Janiak, J. Chem. Soc. Dalton Trans. (2000) 3885.
[28] M. Munakata, T. Kuroda-Sowa, M. Maekawa, A. Hirota, S. Kitagawa, Inorg. Chem. 34 (1995) 2705.
[29] R. Alberto, W. Nef, A. Smith, T.A. Kaden, M. Neuburger, M. Zehnder, A. Frey, U. Abram, P.A. Schubiger, Inorg. Chem. 35 (1996) 3420.
[30] Y. Qi, Y.X. Che, J.M. Zheng, Cryst. Growth Des. 8 (2008) 3602.
[31] G.B. Deacon, R.J. Phillips, Coord. Chem. Rev. 33 (1980) 227.
[32] Y.J. Gao, Z.S. Wu, Z.J. Zhang, Q.J. Xue, Wear 222 (1998) 129.
[33] J.M. Pope, T. Sato, E. Shoji, D.A. Buttry, T. Sotomura, N. Oyama, J. Power Sources 68 (1997) 739.
[34] G.X. Liu, Y.Q. Huang, Q. Chu, T. Okamura, W.Y. Sun, H. Liagn, N. Ueyama, Cryst. Growth Des. 8 (2008) 3233.
[35] P. Lin, R.A. Henderson, R.W. Harrington, W. Clegg, C.D. Wu, X.T. Wu, Inorg. Chem. 43 (2004) 181.
[36] Z. Wang, H.H. Zhang, Y.P. Chen, C.C. Huang, R.Q. Sun, Y.N. Cao, X.H. Yu, J. Solid State Chem. 179 (2006) 1536.
[37] Z.Y. Fu, X.T. Wu, J.C. Dai, S.M. Hu, W.X. Du, H.H. Zhang, R.Q. Sun, Eur. J. Inorg. Chem. (2002) 2730.
[38] L. Yang, F. Bian, S.P. Yan, D.Z. Liao, P. Cheng, Z.H. Jiang, Inorg. Chem. Comm. 6 (2003) 1188.
[39] H. Oshio, E. Ino, I. Mogi, T. Ito, Inorg. Chem. 32 (1993) 5697.
[40] X.M. Chen, Y.X. Tong, Z.T. Xu, T.C.W. Mak, J. Chem. Soc. Dalton Trans. (1995) 4001.
[41] T.K. Maji, S. Sain, G. Mostafa, T.H. Lu, J. Ribas, M. Monfort, N.R. Chaudhuri, Inorg. Chem. 42 (2003) 709.
[42] Y. Cultneh, Y.T. Tesema, B. Ahvazi, T.B. Yisgedu, R.J. Butcher, J.P. Tuchagues, Inorg. Chim. Acta 359 (2006) 4463.
[43] R.H. Wang, D.Q. Yuan, F.L. Jiang, L. Han, S. Gao, M.C. Hong, Eur. J. Inorg. Chem. (2006) 1649.
[44] J.M. Shi, Z. Liu, Y.M. Sun, L. Yi, L.D. Liu, Chem. Phys. 325 (2006) 237.
[45] Y.G. Hong, Y.F. Zhou, D.Q. Yuan, B.L. Wu, F.L. Jiang, M.C. Hong, J. Mol. Struct. 830 (2007) 85.
[46] S.K. Ghosh, J. Ribas, P.K. Bharadwaj, Cryst. Growth Des. 5 (2005) 623.
[47] X.J. Lin, Z. Shen, Y. Song, H.J. Xu, Y.Z. Li, X.Z. You, Inorg. Chim. Acta 358 (2005) 1963.